Nuclear Science and Techniques (2026) 37:122
https://doi.org/10.1007/s41365-026-01940-3

Multireference covariant density functional theory for shape coexistence and isomerism in ^{43}S

En-Fu Zhou[1] · Xian-Ye Wu[2,3] · Jian Xiang[4] · Jiang-Ming Yao[1,5] · Peter Ring[6]

Received: 23 April 2025 / Revised: 31 August 2025 / Accepted: 5 September 2025 / Published online: 11 April 2026

Abstract
We present a new development in the multireference covariant density functional theory (MR-CDFT) for the low-lying states of odd-mass nuclei by mixing configurations with different intrinsic quadrupole shapes and different K quantum numbers. All configurations are projected onto the good particle numbers and angular momenta. The success of this newly developed framework is illustrated in its application to the low-lying states of ^{43}S near the neutron magic number $N = 28$ with shape coexistence. Our results indicate that the ground state, $3/2^-_1$, is predominantly composed of the intruder prolate one-quasiparticle (1qp) configuration $\nu 1/2^-[321]$. In contrast, the $7/2^-_1$ state is identified as a high-K isomer, primarily built on the prolate 1qp configuration $\nu 7/2^-[303]$. Additionally, the $3/2^-_2$ state is found to be an admixture dominated by an oblate configuration with $K^\pi = 1/2^-$, along with a small contribution from a prolate configuration with $K^\pi = 3/2^-$. These results demonstrate the capability of MR-CDFT to capture the intricate interplay among shape coexistence, configuration mixing, and isomerism in the low-energy structure of odd-mass nuclei around $N = 28$, without invoking triaxiality.

Keywords Nuclear density functional theory and extensions · Collective levels · Generator coordinate method · Quantum number projection

This work was partially supported by the National Natural Science Foundation of China (Nos. 12465020, 12005802, 12375119, and 12141501), the Guangdong Basic and Applied Basic Research Foundation (2023A1515010936), the Fundamental Research Funds for the Central Universities, Sun Yat-sen University, and the Deutsche Forschungsgemeinschaft (DFG, German Research Foundation) under Germany's Excellence Strategy – EXC-2094-390783311, ORIGINS.

✉ Xian-Ye Wu
xywu@jxnu.edu.cn

✉ Jian Xiang
jxiang@cqnu.edu.cn

✉ Jiang-Ming Yao
yaojm8@sysu.edu.cn

✉ Peter Ring
peter.ring@tum.de

[1] School of Physics and Astronomy, Sun Yat-sen University, Zhuhai 519082, China

[2] College of Physics and Communication Electronics, Jiangxi Normal University, Nanchang 330022, China

[3] Jiangxi Provincial Key Laboratory of Advanced Electronic Materials and Devices, Nanchang 330022, China

[4] College of Physics and Electronic Engineering, Chongqing Normal University, Chongqing 401331, China

[5] Guangdong Provincial Key Laboratory of Quantum Metrology and Sensing, Sun Yat-Sen University, Zhuhai 519082, China

[6] Physik Department, Technische Universität München, Garching 85748, Germany

1 Introduction

The development of radioactive ion beam facilities [1–3] has significantly advanced nuclear physics research, enabling studies of nuclei far from the β-stability line, where the evolution of the nuclear shell structure and the emergence of exotic excitation modes have garnered considerable attention [4–7]. A striking example is the evolution of the $N = 28$ shell gap, a magic number that arises from strong spin-orbit coupling in the single-nucleon potential [8, 9], which drives the $f_{7/2}$ orbital significantly lower than the $p_{3/2}$ orbital. Experimental data reveal a gradual weakening of the $N = 28$ shell gap in isotones lighter than ^{48}Ca. For instance, measurements of the β-decay half-lives of ^{44}S and ^{45}Cl revealed deviations from shell-model predictions based on spherical configurations [10], indicating the weakening of the $N = 28$ shell effect. Subsequent Coulomb excitation experiments observed low excitation energies of the 2_1^+ states and enhanced electric quadrupole transition strengths $B(E2;0_1^+ \to 2_1^+)$ in ^{40,42,44}S [11, 12]. Similar behavior has been reported in neighboring nuclei, such as ^{42}Si [13–15] and ^{40}Mg [16]. These observations indicate the onset of strong quadrupole collectivity in neutron-rich $N = 28$ isotones with proton number $Z < 18$, leading to the crossing of the $\nu 1/2^-[321]$ component of the $2\nu p_{3/2}$ orbital with the $\nu 7/2^-[303]$ component of the $1\nu f_{7/2}$ orbital. Consequently, several near-degenerate configurations with admixtures of $1f_{7/2}$ and $2p_{3/2}$ orbitals coexist at similar energies within these nuclei. In the case of ^{44}S, two coexisting low-lying 0^+ states have been observed [17], suggesting a spherical-deformed shape coexistence. The onset of a deformed ground state in ^{44}S is supported by quantum number-projected generator coordinate method (GCM) studies based on the Gogny force [18, 19] and a collective Hamiltonian study based on a relativistic energy density functional (EDF) [20]. These two theoretical studies reveal a general trend in shape evolution, that is, the predominant shape transitions from a γ-soft, moderately deformed configuration with $\beta_2 \in [0.20, 0.30]$ to a strongly prolate shape with $\beta_2 \in [0.35, 0.45]$ as the angular momentum increases up to $J = 4$ in the ground state band. This rotational band coexists with a strongly prolate-deformed 0_2^+ state characterized by $\beta_2 \in [0.35, 0.45]$. The specific deformation parameter β_2 of the dominant configuration depends on the details of the employed EDF. The two-proton knockout reaction from ^{46}Ar identified the 4_1^+ state as an isomeric state [21], which, in combination with shell-model calculations, was suggested to exhibit a strong prolate deformation. A half-life measurement revealed a hindered $E2$ transition with $B(E2;4_1^+ \to 2_1^+) = 0.61(19)$ W.u. [22], supporting the interpretation of the 4_1^+ state as a $K = 4$ isomer. Shell-model studies further indicate that this state is predominantly characterized by the two-quasiparticle configuration $\nu 1/2^-[321] \otimes \nu 7/2^-[303]$ [23].

The odd-mass neutron-rich sulfur isotope ^{43}S exhibits a more complex low-energy structure than ^{44}S owing to the interplay between the single-particle motion of the unpaired neutron and the collective excitations of the ^{42}S core. The mass measurements, combined with theoretical studies based on the shell model and relativistic mean-field (RMF) theory, suggested the coexistence of a prolate-deformed ground state and an isomeric state in ^{43}S [24]. Subsequent g-factor measurements [25], along with shell-model calculations and the collective Hamiltonian approach based on the Gogny force, determined the spin-parity of the isomeric state as $7/2_1^-$ at an excitation energy of 320.5(5) keV. These studies also established the intruder nature of the ground state with $K = 1/2$ [25], while initially suggesting that the $7/2_1^-$ isomeric state was quasispherical. However, later measurements of the spectroscopic quadrupole moment of the isomeric state yielded $Q_s(7/2_1^-) = 23(3)\, e\,\mathrm{fm}^2$ [26], which was significantly larger than the expected value for a single-particle state. This observation indicates the strong collective nature of the isomeric state, which is further supported by shell-model calculations [26]. The structure of ^{43}S was investigated using antisymmetrized molecular dynamics plus GCM (AMD+GCM), which predicted a prolate-deformed ground state, a triaxially deformed $7/2_1^-$ state, and an oblate-deformed excited band atop the $3/2_2^-$ state at low excitation energy [27]. In contrast, a recent shell-model study suggested that the prolate ground state band coexists with a triaxial band built on the $7/2_1^-$ isomer and an excited prolate structure associated with the $K^\pi = 5/2^-$ deformed orbital [28]. Meanwhile, the angular momentum-projected variation-after-projection (AMP+VAP) approach suggests that the ground state $3/2_1^-$ and the $7/2_1^-$ state are dominated by $K = 1/2$ and $K = 7/2$, respectively, classifying the $7/2_1^-$ state as a high-K isomer [23]. Experimental lifetime measurements of excited states provide the first evidence of a doublet of $(3/2_2^-, 5/2_1^-)$ states. Together with shell-model and AMD calculations, these results suggest the possible existence of three coexisting bands built upon the $3/2_1^-$, $7/2_1^-$, and $3/2_2^-$ states [29]. Furthermore, Coulomb excitation experiments have shown that the intraband $B(E2)$ values for the transitions within the ground state band $3/2_1^-$ and the isomeric band $7/2_1^-$ are large and nearly equal [30], which was also found in the study of the valence space in-medium similarity renormalization group [31].

Over the past decades, covariant density functional theory (CDFT) has achieved remarkable success in various areas of nuclear physics [32–38]. A key advantage of the CDFT is that Lorentz invariance imposes strict constraints on the number of parameters in the EDF. Moreover, the relativistic framework naturally accounts for the spin-orbit interaction, whereas time-odd fields are incorporated without introducing additional free parameters. This characteristic is particularly crucial for accurately describing odd-mass nuclei and their rotating systems. To restore the missing quantum numbers, including particle numbers and angular momentum, in the solution of CDFT and to consider the shape-mixing effect, the multi-reference covariant density functional theory (MR-CDFT) was developed [39–41] and successfully applied to study low-lying spectra in even–even nuclei with either triaxial or octupole shapes [42–45]. The MR-CDFT has also been applied to the studies of neutrinoless double-beta decay [46–51] and the low-lying states of hypernuclei [52–54].

Recently, the MR-CDFT was successfully extended to describe low-lying states in odd-mass nuclei [55]. In this work, we present a new development in the MR-CDFT for the low-lying states of odd-mass nuclei by mixing the configurations not only with different intrinsic quadrupole shapes, but also with different K quantum numbers. All the configurations are projected onto good particle numbers and angular momenta. This newly developed framework offers an alternative and computationally efficient approach to account for the triaxiality effects in nuclear low-lying states, avoiding the need for full three-dimensional angular momentum projection [39], which is numerically demanding. The success of our framework is demonstrated through its application to the low-energy structure of ^{43}S. It is worth noting that a similar idea has been implemented in the projected shell model (PSM) to study the effect of K-mixing on isomeric states in even–even isotopes with $N = 104$ [56], although the effect of shape mixing was not included in that study. Our extended MR-CDFT enables us to identify the dominant mechanism responsible for the formation of the isomeric state, shedding new light on the interplay among shape coexistence, K-mixing, and isomerism in the low-energy structure of odd-mass nuclei.

The remainder of this paper is organized as follows. In Sect. 2, we present the extended framework of MR-CDFT for odd-mass nuclei. The results of the calculations for ^{43}S are discussed in Sect. 3. The conclusions of this study are summarized in Sect. 4.

2 The MR-CDFT for odd-mass nuclei

The MR-CDFT theory for the low-lying states of odd-mass nuclei was introduced in detail in Ref. [55]. Here, we only present a brief description of the extension of this theory, in which the wave functions of low-lying states are constructed as a mixing of configurations with different deformation parameter $\mathbf{q}$ and quantum number K,

$$|\Psi_\alpha^{J\pi}\rangle = \sum_c f_c^{J\alpha\pi} |NZJ\pi;c\rangle. \tag{1}$$

Here, c is a collective label for $(K, \mathbf{q})$, and α distinguishes states with the same angular momentum J. The basis function with quantum numbers $(NZJ\pi)$ is given by

$$|NZJ\pi;c\rangle = \hat{P}^J_{MK}\hat{P}^N\hat{P}^Z|\Phi_\kappa^{(\mathrm{OA})}(\mathbf{q})\rangle, \tag{2}$$

where $\hat{P}^J_{MK}$ and $\hat{P}^{N(Z)}$ are projection operators that select components with angular momentum J and neutron(proton) number $N(Z)$ [57].

The mean-field configurations $|\Phi_\kappa^{(\mathrm{OA})}(\mathbf{q})\rangle$ for odd-mass nuclei are chosen as 1qp states,

$$|\Phi_\kappa^{(\mathrm{OA})}(\mathbf{q})\rangle = \alpha_\kappa^\dagger|\Phi_{(\kappa)}(\mathbf{q})\rangle, \tag{3}$$

where $|\Phi_{(\kappa)}\rangle$ denotes a quasiparticle vacuum state with even number parity obtained through the false quantum vacuum (FQV) scheme [55] in the single reference (SR)-CDFT calculation starting from a relativistic EDF [34, 58]. In this scheme, the time-reversal invariance is preserved [59]. The quasiparticle creation operator $\alpha^\dagger$ switches the number parity to odd. The index κ distinguishes different quasiparticle states. In this study, axial symmetry was assumed. In this case, each configuration is labeled with the quantum numbers K^π, determined by the quantum numbers Ω^π of the blocked orbital. In the configuration mixing calculation, only the lowest energy quasiparticle configuration with a given K^π is included for each deformed configuration. In addition to the configurations employed in Ref. [55], we also mixed the configurations with different K values.

The weight function $f_c^{J\alpha\pi}$ in Eq. (1) is determined by the variational principles that lead to the following Hill–Wheeler–Griffin (HWG) equation [57, 60],

$$\sum_{c'}\left[\mathscr{H}_{cc'}^{NZJ\pi} - E_\alpha^{J\pi}\mathscr{N}_{cc'}^{NZJ\pi}\right]f_{c'}^{J\alpha\pi} = 0, \tag{4}$$

where the Hamiltonian kernel and norm kernel are defined by

$$\mathscr{O}_{cc'}^{NZJ\pi} = \langle NZJ\pi;c|\hat{O}|NZJ\pi;c'\rangle, \tag{5}$$

with the operator $\hat{O}$ representing $\hat{H}$ and 1, respectively. In the present study, based on a covariant EDF, the mixed-density prescription is employed in the evaluation of the Hamiltonian kernel. Details of the calculation of the kernels in Eq. (5) can be found in Ref. [55].

The HWG Eq. (4) for a given set of quantum numbers $(NZJ\pi)$ is solved in the standard way, as discussed in Refs. [40, 57]. This is done by first diagonalizing the norm kernel $\mathscr{N}_{cc'}^{NZJ\pi}$. A new set of basis functions is then constructed using the eigenfunctions of the norm kernel with eigenvalues larger than a pre-chosen cutoff value, which removes the possible redundancy in the original basis. The Hamiltonian is diagonalized using this new basis. In this way, the energies $E_\alpha^{J\pi}$ and the mixing weights $f_c^{J\alpha\pi}$ of the nuclear states $|\Psi_\alpha^{J\pi}\rangle$ can be obtained. Since the basis functions $|NZJ\pi;c\rangle$ are nonorthogonal to each other, one usually introduces the collective wave function $g_\alpha^{J\pi}(K,\mathbf{q})$ as below

$$g_\alpha^{J\pi}(K,\mathbf{q}) = \sum_{c'}(\mathscr{N}^{1/2})_{c,c'}^{NZJ\pi} f_{c'}^{J\alpha\pi}, \tag{6}$$

which fulfills the normalization condition. The distribution of $g_\alpha^{J\pi}(K,\mathbf{q})$ over K and $\mathbf{q}$ reflects the contribution of each basis function to the nuclear state $|\Psi_\alpha^{J\pi}\rangle$. With the mixing weight $f_c^{J\alpha\pi}$, it is straightforward to determine the observables of nuclear low-lying states, including the electric quadrupole moment Q_s, magnetic dipole moment μ, and the $E2$ and $M1$ transition strengths. The strength of the $E\lambda(M\lambda)$ transition from the initial state $|\Psi_{\alpha_i}^{J_i\pi_i}\rangle$ to the final state $|\Psi_{\alpha_f}^{J_f\pi_f}\rangle$ is determined by

$$B(T\lambda, J_i\alpha_i\pi_i \to J_f\alpha_f\pi_f) = \frac{1}{2J_i+1} \times \left| \sum_{c_f,c_i} f_{c_i}^{J_i\alpha_i\pi_i} f_{c_f}^{J_f\alpha_f\pi_f} \langle NZJ_f\pi_f, c_f||\hat{T}_\lambda||NZJ_i\pi_i, c_i\rangle \right|^2, \tag{7}$$

where the configuration-dependent reduced matrix element is simplified as follows,

$$\begin{aligned}\langle NZJ_f\pi_f;c_f||\hat{T}_\lambda||NZJ_i\pi_i;c_i\rangle &= \delta_{\pi_f\pi_i,(-1)^L}(-1)^{J_f-K_f}\frac{\hat{J}_i^2\hat{J}_f^2}{8\pi^2}\sum_{\nu M}\begin{pmatrix} J_f & \lambda & J_i \\ -K_f & \nu & M\end{pmatrix} \\ &\times \int d\Omega D_{MK_i}^{J_i*}(\Omega)\langle\Phi_{\kappa_f}^{(OA)}(\mathbf{q}_f)|\hat{T}_{\lambda\nu}\hat{R}(\Omega)\hat{P}^Z\hat{P}^N\hat{P}^{\pi_i}|\Phi_{\kappa_i}^{(OA)}(\mathbf{q}_i)\rangle,\end{aligned} \tag{8}$$

where $\hat{T}_{\lambda\nu}$ represents either an electric ($L = \lambda$) or magnetic ($L = \lambda + 1$) multiple operator and $\hat{J} = \sqrt{2J+1}$. The detailed formulas can be found in Ref. [55].

3 Results and discussion

In the calculation of the mean-field configurations, Dirac spinors for single nucleons were solved using a harmonic oscillator (HO) basis with a major shell number of $N_{sh} = 10$, with frequency $\hbar\omega_{HO} = 41A^{-1/3}$ MeV. Pairing correlations between nucleons are treated within the BCS approximation using a density-independent δ force with a smooth cutoff [39, 61]. The PC-PK1 parameterization was employed for the relativistic EDF [58]. Even though PC-PK1 is not the best EDF, it is very successful in various nuclear structure studies [34]. Therefore, it is natural to continue using this EDF parameter set in the illustrative study of the low-lying states of ^{43}S. In the calculation of the projected kernels $\mathcal{O}_{cc'}^{NZJ\pi}$, the number of mesh points in the interval $[0,\pi]$ for the rotation angle β and the gauge angle φ were chosen as $N_\beta = 12$ and $N_\varphi = 7$, respectively. These values are sufficient to achieve convergent results for ^{43}S.

Figure 1a presents the energies of mean-field states $|\Phi_{(\kappa)}(\mathbf{q})\rangle$ from the SR-CDFT calculation based on the FQV scheme [55] as a function of the quadrupole deformation parameter $\mathbf{q} = \beta_2$. A pronounced energy minimum appears

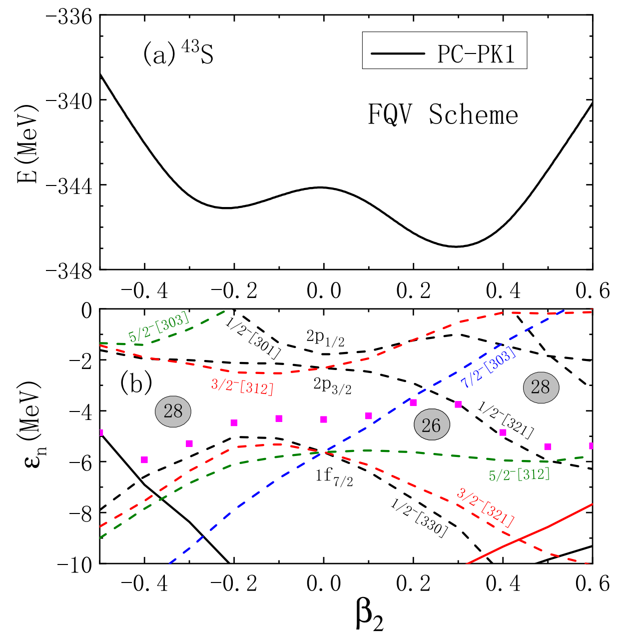

Fig. 1 (Color online) **a** Total energy of the mean-field states for ^{43}S from the SR-CDFT calculation based on the FQV scheme, as a function of the quadrupole deformation parameter β_2. **b** Nilsson diagram for neutrons in ^{43}S, with the Fermi energies indicated by the pink squares. The numbers around the lines are the Nilsson quantum numbers $\Omega^\pi[Nn_zm_\ell]$ [57]

on the prolate side with $\beta_2 \simeq 0.3$, with a second minimum on the oblate side with $\beta_2 \simeq -0.2$, suggesting that ^{43}S may exhibit coexisting prolate and oblate shapes in its low-lying states. This phenomenon can be understood from the Nilsson diagram of neutrons in ^{43}S, as shown in Fig. 1b. One can observe large shell gaps or low-level densities on both prolate and oblate sides around the Fermi energy. Moreover, the downward $\nu1/2^-[321]$ component of the $2\nu p_{3/2}$ orbital crosses with the upward $\nu7/2^-[303]$ component of the $1\nu f_{7/2}$ orbital at $\beta_2 \simeq 0.22$ around the Fermi energy. This crossing leads to the population of valence neutrons from $\nu7/2^-[303]$ to $\nu1/2^-[321]$. This result is consistent with the AMD+GCM calculation [27]. On the oblate side, the $N = 28$ shell gap increases with $|\beta_2|$.

The wave functions of the mean-field states $|\Phi_{(\kappa)}(\beta_2)\rangle$ in Fig. 1a do not preserve the particle numbers or total angular momentum. By applying quantum number projection operators onto the 1qp configurations with $K^\pi = 1/2^-, 3/2^-, 5/2^-$, and $7/2^-$, c.f. Eqs. (2) and (3), one obtains the energies of the symmetry-conserved 1qp states in ^{43}S, as displayed in Fig. 2. The low-lying states from the shape-mixing calculation are plotted at their mean quadrupole deformation $\bar{\beta}_2^{J\pi\alpha}$, which is defined as

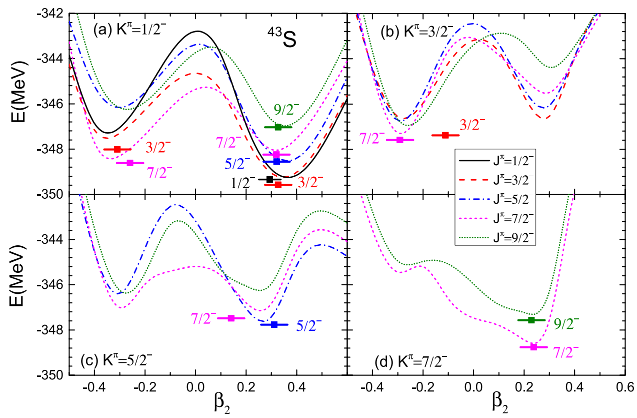

Fig. 2 (Color online) Energies of symmetry-conserving 1qp states with different angular momenta J in ^{43}S for **a** $K^\pi = 1/2^-$, **b** $K^\pi = 3/2^-$, **c** $K^\pi = 5/2^-$, and **d** $K^\pi = 7/2^-$, as functions of the quadrupole deformation parameter β_2. The discrete low-lying states obtained by mixing configurations of different shapes, but with fixed K^π values, within the GCM framework are shown at their mean quadrupole deformation $\bar{\beta}_2^{J\pi\alpha}$, as defined in Eq. (9)

$$\bar{\beta}_2^{J\pi\alpha}(K^\pi) = \sum_{\beta_2} |g_\alpha^{J\pi}(K, \beta_2)|^2 \beta_2. \tag{9}$$

The energies of symmetry-conserving states with angular momentum J increasing from 1/2 to 9/2, projected out from the configurations with $K^\pi = 1/2^-$ as a function of the quadrupole deformation β_2, are displayed in Fig. 2a. Similar to the energy curve of the mean-field calculation shown in Fig. 1a, all the projected energy curves present two energy minima on the prolate and oblate sides, with $|\beta_2| \simeq 0.3$. It is interesting to note the change in the energy ordering of states with different angular momenta as a function of the deformation, as shown in Fig. 2a. For configurations with $\beta_2 > 0.4$, the energies of the projected states with $\Delta J = 1$ follow the ordering of $(1/2^-, 3/2^-, 5/2^-, 7/2^-, 9/2^-)$, which are consistent with the *strong* coupling limit of the particle-rotor model (PRM) [57]. In contrast, for weakly deformed configurations with $\beta_2 < 0.3$, the $1/2^-$ state rises rapidly from the bottom as β_2 decreases toward zero. When only the configurations of the oblate energy minima are considered, the energy ordering is $(7/2^-, 3/2^-, 1/2^-, 9/2^-, 5/2^-)$. After mixing the configurations with different shapes but the same quantum numbers $K^\pi = 1/2^-$, the yrast states with the energy ordering of $(3/2^-, 1/2^-, 5/2^-, 7/2^-)$ are mainly located around $\beta_2 = 0.3$.

Figure 2b, c, and d displays the energies of symmetry-conserving states with $J \geq K$, projected out from the configurations with $K^\pi = 3/2^-, 5/2^-$, and $7/2^-$, as well as the two lowest energy states from the shape-mixing calculation. It can be seen that the energy level $7/2^-$ dominated by the prolate configuration with $K^\pi = 7/2^-$ is the yrast state among all the $J^\pi = 7/2^-$ states. All states with the same quantum numbers J^π, but with different K^π can be mixed. The final states from the MR-CDFT calculation by mixing 1qp configurations with different deformations and K^π values are plotted in Fig. 3b. The distributions of the collective wave functions for the first two $3/2^-, 5/2^-$, and $7/2^-$ states are shown in the bottom panels of Fig. 3. It is seen that the main features of the measured low-lying states of ^{43}S, cf. Fig. 3a, are reasonably well reproduced only in the MR-CDFT calculations with the mixing of these two types of configurations.

Here, we summarize the main findings of the MR-CDFT study based on Fig. 3. The ground state $(3/2_1^-)$ of ^{43}S is predominantly characterized by a prolate-deformed configuration, $\nu 1/2^-[321]$, with $K^\pi = 1/2^-$. This can be understood from Fig. 2a, which shows the potential energy surfaces with $J^\pi = 3/2^-$ projected from the configurations with $K^\pi = 1/2^-$ present a pronounced global energy minimum around $\beta_2 = 0.35$ and a second minimum around $\beta_2 = -0.35$. These energies are much lower than those with $J^\pi = 3/2^-$ but projected from the configurations with $K^\pi = 3/2^-$. Thus, it is expected that the lowest $J^\pi = 3/2^-$ state is dominated by configurations with $K^\pi = 1/2^-$ instead of those with $K^\pi = 3/2^-$. In contrast, the $3/2_2^-$ state is dominated by an oblate configuration with $\beta_2 \simeq -0.3$ and $K^\pi = 1/2^-$, with a small admixture of a prolate configuration having $K^\pi = 3/2^-$. In the AMD+GCM calculation [27], the $3/2_2^-$ state is dominated by an oblate configuration with $K^\pi = 3/2^-$, followed by the $5/2_2^-$ and $7/2_3^-$ states, forming an oblate rotational band. As shown in Fig. 3b, we predict a strong $E2$ transition between the $5/2_2^-$ and $7/2_3^-$ states, whereas the $E2$ transition from the $5/2_2^-$ to the $3/2_2^-$ state is much weaker. This behavior can be understood from Fig. 3g, which shows that the $5/2_2^-$ state is dominated by a prolate-deformed configuration with $K^\pi = 5/2^-$, in contrast to the oblate structure of the $3/2_2^-$ state.

The first excited state of ^{43}S, $1/2_1^-$, shares a similar predominant configuration with the ground state and exhibits a strong $E2$ transition to the ground state. The MR-CDFT predicts $B(E2;1/2_1^- \to 3/2_1^-) = 144\, e^2\,\text{fm}^4$, as well as a sizable $M1$ transition, with $B(M1;1/2_1^- \to 3/2_1^-) = 0.45\ \mu_N^2$, as shown in Fig. 3b. In the AMD+GCM [27], these numbers are 180 e^2 fm^4 and $0.34\mu_N^2$, respectively. The value of $B(E2;1/2_1^- \to 3/2_1^-)$ has not yet been measured, but experimental data are available for $B(M1;1/2_1^- \to 3/2_1^-) = 1.2(3)$ μ_N^2 [29], which is underestimated by both methods. We find that this underestimation is due to the extension of the wave function of the $3/2_1^-$ state into the region of large prolate deformation with $\beta_2 > 0.4$, as shown in Fig. 3d. Moreover, we observe two $\Delta J = 2$ rotational bands, namely $(3/2_1^-, 7/2_2^-, 11/2_1^-)$ and $(1/2_1^-, 5/2_1^-, 9/2_2^-)$, which are connected by strong $E2$ transitions. The predicted $B(E2;7/2_2^- \to 3/2_1^-) = 59\ e^2\ \text{fm}^4$ is slightly larger than the data 46(9) e^2 fm^4 [30]. All these states are predominantly characterized by the prolate-deformed configuration

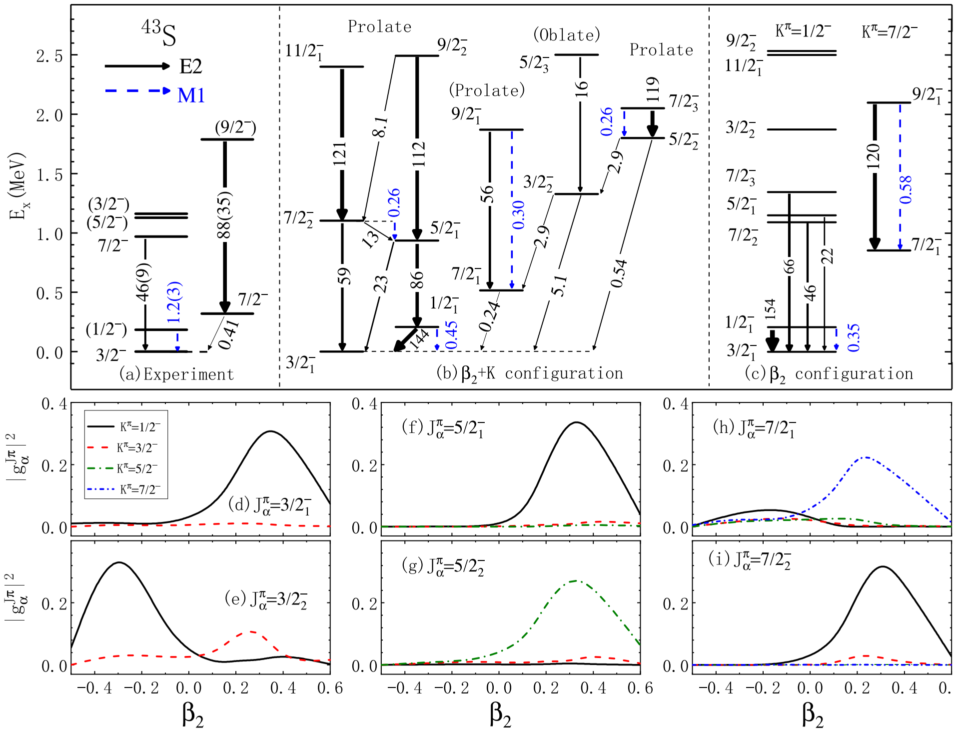

Fig. 3 (Color online) Energy spectra and collective wave functions of low-lying states in ^{43}S from MR-CDFT calculations. Experimental data [25, 30] are displayed in panel (**a**). Panel **b** shows the results including configuration mixing among states with different shapes and K values, while panel **c** presents the results of calculations by mixing only the configurations with different quadrupole deformations β_2, where the blocked orbitals correspond to $K^\pi = 1/2^-$ and $7/2^-$, respectively. The black and blue arrows indicate the $B(E2)$ values (in units of e^2 fm ^{4}) and $B(M1)$ values (in units of μ_N^2), respectively. The states dominated by a prolate (oblate) configuration, with a small admixture of oblate (prolate) components, are labeled as "(Prolate)" and "(Oblate)", respectively. The distributions of the collective wave functions $|g_\alpha^{J\pi}(K,\beta_2)|^2$ for the first two states with $J = 3/2$, 5/2, and 7/2 are shown in panels (**d**, **e**), (**f**, **g**), and (**h**, **i**), respectively

$\nu 1/2^-[321]$, originating from the spherical $\nu p_{3/2}$ orbital, with deformation $\beta_2 \simeq 0.3$ and $K^\pi = 1/2^-$, as shown in Fig. 1. The energy ordering of the $(3/2^-_1, 7/2^-_2, 11/2^-_1)$ sequence follows the *weak* coupling limit of the PRM [57], which predicts a parabolic energy pattern with a minimum at $J \simeq j = 3/2$.

Figure 3h shows that the $7/2^-_1$ state is dominated by the prolate-deformed configuration $\nu 7/2^-[303]$ with $\beta_2 \simeq 0.22$ and $K^\pi = 7/2^-$. Consequently, the decay of the $7/2^-_1$ state to the ground state $(3/2^-)$ is strongly quenched because of $\Delta K = 3$. Quantitatively, the predicted $B(E2;7/2^-_1 \to 3/2^-_1) = 0.24\ e^2$ fm^4, compared to the data 0.41 e^2 fm^4 [25]. Consequently, the $7/2^-_1$ state was classified as a high-K isomer state, consistent with the conclusions of previous studies [23, 28]. A comparison between Fig. 3b and c reveals that the excitation energy of the $7/2^-_1$ state decreases significantly and becomes closer to the experimental value after incorporating 1qp configuration mixing with different K^π values. In contrast, the $7/2^-_2$ oblate nature in Fig. 3c is pushed very high and is not shown in Fig. 3b. As shown in Fig. 3h, the isomeric $7/2^-_1$ state also contains a small admixture of an oblate configuration with $K^\pi = 1/2^-$. The remaining discrepancy is expected to be reduced by explicitly including the triaxial deformation effect, as suggested by the AMD+GCM calculation [27].

Table 1 lists the spectroscopic quadrupole moments Q_s and magnetic dipole moments μ for ^{43}S obtained from the MR-CDFT calculations with 1qp configuration mixing involving different quadrupole deformations β_2 and K^π values, in comparison with the results of AMD+GCM calculations [27] and available data for the isomer state with $Q_s(7/2^-_1) = 23(3)\ e$ fm^2 and $\mu(7/2^-_1) = -1.110(14)\ \mu_N$. Overall, the results from MR-CDFT and AMD+GCM were similar, with both models reasonably reproducing the experimental data. Quantitatively, the Q_s values of the states in the ground state band predicted by MR-CDFT are slightly smaller than those from AMD+GCM. Notably, the magnetic moments of the $1/2^-_1$ and $7/2^-_2$ states obtained using MR-CDFT are only approximately half of the values predicted by AMD+GCM. In particular, a significant discrepancy was found in the prediction for the $5/2^-_2$ state. Although the AMD+GCM calculation suggests that this state is dominated by an oblate configuration, the MR-CDFT result favors a prolate deformation, consistent with

Table 1 The spectroscopic quadrupole moments $Q_s(J^\pi_\alpha)$ and magnetic dipole moments $\mu(J^\pi_\alpha)$ for ^{43}S based on MR-CDFT calculations, in comparison with the prediction of AMD+GCM calculations [27] and data [26]

J^π_α	$Q_s(e\,\mathrm{fm}^2)$			$\mu(\mu_N)$		
	Exp.	MR-CDFT	AMD	Exp.	MR-CDFT	AMD
$1/2^-_1$	–	–	–	–	0.48	0.71
$3/2^-_1$	–	−13.0	−13.2	–	−0.76	−0.60
$5/2^-_1$	–	−17.4	−20.1	–	1.49	1.45
$7/2^-_2$	–	−18.9	−22.0	–	−0.12	−0.24
$9/2^-_2$	–	−24.1	−21.4	–	2.20	1.26
$3/2^-_2$	–	9.2	12.1	–	−0.54	−0.82
$5/2^-_2$	–	18.1	−7.0	–	−0.85	0.14
$5/2^-_3$	–	−4.0	–	–	0.18	–
$7/2^-_1$	23(3)	20.9	26.1	−1.110(14)	−0.93	−1.08
$9/2^-_1$	–	4.9	7.3	–	0.08	−0.19

the latest shell-model calculations [28]. According to the MR-CDFT calculations, the $5/2^-_2$ state primarily originates from blocking the $\Omega^\pi = 5/2^-$ component of the spherical $\nu f7/2$ state at a deformation of $\beta_2 = 0.3$, as evidenced by the collective wave function shown in Fig. 3g. This state serves as the bandhead of a rotational band built on a prolate shape, as illustrated in the low-lying spectrum of ^{43}S in Fig. 3b. In contrast, AMD+GCM calculations [27] indicate that this excited band is dominated by the oblate component $\Omega^\pi = 3/2^-$ of the spherical $\nu f_{7/2}$ state. Interestingly, the MR-CDFT calculations also predict an oblate $5/2^-_3$ arising from blocking the $\Omega^\pi = 3/2^-$ orbital of the $\nu f_{7/2}$ state with an excitation energy of approximately 2.5 MeV. This state has a different structure from the oblate $3/2^-_2$ state, which is dominated by the configuration of $K^\pi = 1/2^-$, see Fig. 3e. Moreover, as seen from Table 1, the spectroscopic quadrupole moment Q_s and magnetic dipole moment μ of our $5/2^-_3$ state are close to those of the $5/2^-_2$ state predicted by the AMD+GCM approach. Whether the second $5/2^-_2$ state is predominantly prolate or oblate can be clarified by future measurements of its electromagnetic properties.

4 Summary

In this study, we extended the multireference covariant density functional theory (MR-CDFT) for odd-mass nuclei by incorporating particle number and angular momentum projections, along with the simultaneous mixing of quasiparticle configurations characterized by different quadrupole deformations and K quantum numbers. The effectiveness of this extended framework is demonstrated through its application to the low-lying states of ^{43}S, where the available experimental data on the energy spectra, electric quadrupole and magnetic dipole transition strengths, and electromagnetic moments are reproduced with reasonable accuracy.

Our calculations reveal a pair of prolate rotational bands with $\Delta J = 2$, built on the ground state configuration $\nu 1/2^-[321]$ ($K^\pi = 1/2^-$), consistent with the weak-coupling limit of the particle-rotor model. A rotational band is also found based on the $\nu 7/2^-[303]$ ($K^\pi = 7/2^-$) configuration, corresponding to the isomeric $7/2^-_1$ state, which is identified as a high-K isomer. These findings are generally consistent with those from AMD+GCM and shell-model calculations, supporting the erosion of the $N = 28$ shell gap. We also identify a $3/2^-_2$ state dominated by an oblate configuration with $K^\pi = 1/2^-$, where the valence neutron occupies the $\nu 1/2^-[330]$ orbital. Furthermore, we predict $5/2^-_2$ and $5/2^-_3$ states, which are dominated by a prolate configuration with $K^\pi = 5/2^-$ and an oblate configuration with $K^\pi = 3/2^-$, respectively. This result is slightly different from the predictions of AMD+GCM with explicit inclusion of triaxiality, which suggests that the $5/2^-_2$ state is dominated by the oblate configuration with $K^\pi = 3/2^-$. This discrepancy calls for further clarification through additional lifetime measurements.

It is worth emphasizing that the present framework is based on axially deformed quasiparticle configurations, with triaxial effects partially incorporated through explicit K-mixing. This makes it a computationally efficient alternative to previous approaches that fully account for triaxiality and require a three-dimensional angular momentum projection. The improved efficiency enables systematic beyond-mean-field studies of shape coexistence and isomeric states in heavy deformed odd-mass nuclei, such as ^{229}Th.

Author contributions All authors contributed to the study conception and design. Material preparation, data collection, and analysis were performed by En-Fu Zhou, Xian-Ye Wu, Jian Xiang, and Jiang-Ming Yao. The first draft of the manuscript was written by En-Fu Zhou, and all authors commented on previous versions of the manuscript. All authors read and approved the final manuscript.

Data availability The data that support the findings of this study are openly available in Science Data Bank at https://cstr.cn/31253.11.sciencedb.35627 and https://doi.org/10.57760/sciencedb.35627.

Declarations

Conflict of interest The authors declare that they have no conflict of interest.

References

1. Y. Yano, The RIKEN RI beam factory project: a status report. Nucl. Instrum. Meth. B **261**, 1009–1013 (2007). https://doi.org/10.1016/j.nimb.2007.04.174
2. T. Glasmacher, B. Sherrill, W. Nazarewicz et al., Facility for rare isotope beams update for nuclear physics news. Nucl. Phys. News **27**, 28–33 (2017). https://doi.org/10.1080/10619127.2017.1317176
3. Y. Ye, X. Yang, H. Sakurai et al., Physics of exotic nuclei. Nat. Rev. Phys. **7**, 21–37 (2025). https://doi.org/10.1038/s42254-024-00782-5
4. E. Caurier, G. Martinez-Pinedo, F. Nowacki et al., The shell model as unified view of nuclear structure. Rev. Mod. Phys. **77**, 427–488 (2005). https://doi.org/10.1103/RevModPhys.77.427
5. O. Sorlin, M.G. Porquet, Nuclear magic numbers: new features far from stability. Prog. Part. Nucl. Phys. **61**, 602–673 (2008). https://doi.org/10.1016/j.ppnp.2008.05.001
6. T. Otsuka, A. Gade, O. Sorlin et al., Evolution of shell structure in exotic nuclei. Rev. Mod. Phys. **92**, 015002 (2020). https://doi.org/10.1103/RevModPhys.92.015002
7. N. Tsunoda, T. Otsuka, K. Takayanagi et al., The impact of nuclear shape on the emergence of the neutron dripline. Nature **587**, 66–71 (2020). https://doi.org/10.1038/s41586-020-2848-x
8. M.G. Mayer, On closed shells in nuclei. II. Phys. Rev. **75**, 1969–1970 (1949). https://doi.org/10.1103/PhysRev.75.1969
9. O. Haxel, J.H.D. Jensen, H.E. Suess, On the magic numbers in nuclear structure. Phys. Rev. **75**, 1766–1766 (1949). https://doi.org/10.1103/PhysRev.75.1766.2
10. O. Sorlin, D. Guillemaud-Mueller, A.C. Mueller et al., Decay properties of exotic $N \sim 28$ S and Cl nuclei and the ^{48}Ca/^{46}Ca abundance ratio. Phys. Rev. C **47**, 2941–2953 (1993). https://doi.org/10.1103/PhysRevC.47.2941
11. H. Scheit, T. Glasmacher, B.A. Brown et al., New region of deformation: the neutron-rich sulfur isotopes. Phys. Rev. Lett. **77**, 3967–3970 (1996). https://doi.org/10.1103/PhysRevLett.77.3967
12. T. Glasmacher, B.A. Brown, M.J. Chromik et al., Collectivity in ^{44}S. Phys. Lett. B **395**, 163–168 (1997). https://doi.org/10.1016/S0370-2693(97)00077-4
13. A. Gade, B.A. Brown, J.A. Tostevin et al., Is the structure of ^{42}Si understood? Phys. Rev. Lett. **122**, 222501 (2019). https://doi.org/10.1103/PhysRevLett.122.222501
14. B. Bastin, S. Grévy, D. Sohler et al., Collapse of the N=28 shell closure in ^{42}Si. Phys. Rev. Lett. **99**, 022503 (2007). https://doi.org/10.1103/PhysRevLett.99.022503
15. S. Takeuchi, M. Matsushita, N. Aoi et al., Well-developed deformation in ^{42}Si. Phys. Rev. Lett. **109**, 182501 (2012). https://doi.org/10.1103/PhysRevLett.109.182501
16. H.L. Crawford, P. Fallon, A. O. Macchiavelli et al., First spectroscopy of the near drip-line nucleus ^{40}Mg. Phys. Rev. Lett. **122**, 052501 (2019). https://doi.org/10.1103/PhysRevLett.122.052501
17. S. Grévy, F. Negoita, I. Stefan et al., Observation of the 0+2 state in ^{44}S. Europ. Phys. J. **25**, 111 (2005). https://doi.org/10.1140/epjad/i2005-06-179-8
18. T.R. Rodriguez, J.L. Egido, Configuration mixing description of the nucleus ^{44}S. Phys. Rev. C **84**, 051307 (2011). https://doi.org/10.1103/PhysRevC.84.051307
19. J.L. Egido, M. Borrajo, T.R. Rodríguez, Collective and single-particle motion in beyond mean field approaches. Phys. Rev. Lett. **116**, 052502 (2016). https://doi.org/10.1103/PhysRevLett.116.052502
20. Z.P. Li, J.M. Yao, D. Vretenar et al., Energy density functional analysis of shape evolution in N=28 isotones. Phys. Rev. C **84**, 054304 (2011). https://doi.org/10.1103/PhysRevC.84.054304
21. D. Santiago-Gonzalez, I. Wiedenhöver, V. Abramkina et al., Triple configuration coexistence in ^{44}S. Phys. Rev. C **83**, 061305 (2011). https://doi.org/10.1103/PhysRevC.83.061305
22. J.J. Parker, I. Wiedenhöver, P. D. Cottle et al., Isomeric character of the lowest observed 4^+ state in ^{44}S. Phys. Rev. Lett. **118**, 052501 (2017). https://doi.org/10.1103/PhysRevLett.118.052501
23. Y. Utsuno, N. Shimizu, T. Otsuka et al., Nature of isomerism in exotic sulfur isotopes. Phys. Rev. Lett. **114**, 032501 (2015). https://doi.org/10.1103/PhysRevLett.114.032501
24. F. Sarazin, H. Savajols, W. Mittig et al., Shape coexistence and the $N = 28$ shell closure far from stability. Phys. Rev. Lett. **84**, 5062–5065 (2000). https://doi.org/10.1103/PhysRevLett.84.5062
25. L. Gaudefroy, J. M. Daugas, M. Hass et al., Shell erosion and shape coexistence in ^{43}S. Phys. Rev. Lett. **102**, 092501 (2009). https://doi.org/10.1103/PhysRevLett.102.092501
26. R. Chevrier, J.M. Daugas, L. Gaudefroy et al., Is the $7/2^-_1$ isomer state of ^{43}S spherical? Phys. Rev. Lett. **108**, 162501 (2012). https://doi.org/10.1103/PhysRevLett.108.162501
27. M. Kimura, Y. Taniguchi, Y. Kanada-En'yo et al., Prolate, oblate, and triaxial shape coexistence, and the lost magicity of $N = 28$ in ^{43}S. Phys. Rev. C **87**, 011301 (2013). https://doi.org/10.1103/PhysRevC.87.011301
28. R. Chevrier, L. Gaudefroy, Shell model structure of ^{43}S and ^{44}S re-examined. Phys. Rev. C **89**, 051301 (2014). https://doi.org/10.1103/PhysRevC.89.051301
29. T. Mijatović, N. Kobayashi, H. Iwasaki et al., Lifetime measurements and triple coexisting band structure in ^{43}S. Phys. Rev. Lett. **121**, 012501 (2018). https://doi.org/10.1103/PhysRevLett.121.012501
30. B. Longfellow, D. Weisshaar, A. Gade et al., Shape changes in the N=28 Island of inversion: collective structures built on configuration-coexisting states in ^{43}S. Phys. Rev. Lett. **125**, 232501 (2020). https://doi.org/10.1103/PhysRevLett.125.232501
31. Q. Yuan, J.G. Li, W. Zuo, Ab initio calculations for configuration-coexisting states in ^{45}S: an extension from ^{43}S. Phys. Rev. C **109**, L041301 (2024). https://doi.org/10.1103/PhysRevC.109.L041301
32. D. Vretenar, A. Afanasjev, G. Lalazissis et al., Relativistic hartree–bogoliubov theory: static and dynamic aspects of exotic nuclear structure. Phys. Rep. **409**, 101–259 (2005). https://doi.org/10.1016/j.physrep.2004.10.001
33. J. Meng, H. Toki, S.G. Zhou et al., Relativistic continuum Hartree Bogoliubov theory for ground state properties of exotic nuclei. Prog. Part. Nucl. Phys. **57**, 470–563 (2006). https://doi.org/10.1016/j.ppnp.2005.06.001
34. J. Meng, *Relativistic Density Functional for Nuclear Structure* (World Scientific, Singapore, 2016)
35. K.P. Geng, P.X. Du, J. Li et al., Calculation of microscopic nuclear level densities based on covariant density functional theory. Nucl. Sci. Tech. **34**, 141 (2023). https://doi.org/10.1007/s41365-023-01298-w
36. W. Zhang, W. Gao, G.T. Zhang et al., Level density of odd-A nuclei at saddle point. Nucl. Sci. Tech. **34**, 124 (2023). https://doi.org/10.1007/s41365-023-01270-8
37. Z.K. Li, Y.Y. Wang, Robustness of the octupole collectivity in ^{144}Ba within the cranking covariant density functional theory in

3D lattice. Nucl. Sci. Tech. **35**, 139 (2024). https://doi.org/10.1007/s41365-024-01532-z

38. Y.M. Wang, Q.B. Chen, Moments of inertia of triaxial nuclei in covariant density functional theory. Nucl. Sci. Tech. **35**, 183 (2024). https://doi.org/10.1007/s41365-024-01552-9
39. J.M. Yao, J. Meng, P. Ring et al., Three-dimensional angular momentum projection in relativistic mean-field theory. Phys. Rev. C **79**, 044312 (2009). https://doi.org/10.1103/PhysRevC.79.044312
40. J.M. Yao, J. Meng, P. Ring et al., Configuration mixing of angular-momentum projected triaxial relativistic mean-field wave functions. Phys. Rev. C **81**, 044311 (2010). https://doi.org/10.1103/PhysRevC.81.044311
41. T. Niksic, D. Vretenar, P. Ring, Relativistic nuclear energy density functionals: mean-field and beyond. Prog. Part. Nucl. Phys. **66**, 519–548 (2011). https://doi.org/10.1016/j.ppnp.2011.01.055
42. J.M. Yao, K. Hagino, Z.P. Li et al., Microscopic benchmark study of triaxiality in low-lying states of ^{76}Kr. Phys. Rev. C **89**, 054306 (2014). https://doi.org/10.1103/PhysRevC.89.054306
43. J.M. Yao, E.F. Zhou, Z.P. Li, Beyond relativistic mean-field approach for nuclear octupole excitations. Phys. Rev. C **92**, 041304 (2015). https://doi.org/10.1103/PhysRevC.92.041304
44. E.F. Zhou, J.M. Yao, Generator coordinate method for nuclear octupole excitations: status and perspectives. Int. J. Mod. Phys. E **32**, 2340011 (2023). https://doi.org/10.1142/S0218301323400116
45. X.Y. Wu, J.Z. Cao, K.N. Zhao et al., Static or dynamic pear shapes in radioactive nucleus ^{224}Rn? Nucl. Sci. Tech. **35**, 202 (2024). https://doi.org/10.1007/s41365-024-01578-z
46. L.S. Song, J.M. Yao, P. Ring et al., Relativistic description of nuclear matrix elements in neutrinoless double-β decay. Phys. Rev. C **90**, 054309 (2014). https://doi.org/10.1103/PhysRevC.90.054309
47. L.S. Song, J.M. Yao, P. Ring et al., Nuclear matrix element of neutrinoless double-β decay: relativity and short-range correlations. Phys. Rev. C **95**, 024305 (2017). https://doi.org/10.1103/PhysRevC.95.024305
48. J.M. Yao, L.S. Song, K. Hagino et al., Systematic study of nuclear matrix elements in neutrinoless double-β decay with a beyond-mean-field covariant density functional theory. Phys. Rev. C **91**, 024316 (2015). https://doi.org/10.1103/PhysRevC.91.024316
49. J.M. Yao, J. Meng, Y.F. Niu et al., Beyond-mean-field approaches for nuclear neutrinoless double beta decay in the standard mechanism. Prog. Part. Nucl. Phys. **126**, 103965 (2022). https://doi.org/10.1016/j.ppnp.2022.103965
50. Y. Li, X. Zhang, G. Giacalone et al., Benchmarking nuclear matrix elements of $0\nu\beta\beta$ decay with high-energy nuclear collisions. Phys. Rev. Lett. **135**, 022301 (2025). https://doi.org/10.1103/zymp-tyjj
51. J. Jia, Bridging nuclear physics across energy scales: from neutrinoless double-beta decay to high-energy heavy-ion collisions. Nucl. Sci. Tech. **36**, 207 (2025). https://doi.org/10.1007/s41365-025-01800-6
52. H. Mei, K. Hagino, J.M. Yao, Generator coordinate method for hypernuclear spectroscopy with a covariant density functional. Phys. Rev. C **93**, 011301 (2016). https://doi.org/10.1103/PhysRevC.93.011301
53. H. Xia, X. Wu, H. Mei et al., Beyond mean-field approach for pear-shaped hypernuclei. Sci. China Phys. Mech. Astron. **62**, 42011 (2019). https://doi.org/10.1007/s11433-018-9308-0
54. H. Xia, X. Wu, H. Mei et al., The interplay of single-particle and collective motions in the low-lying states of $^{21}_{\Lambda}$ with quadrupole-octupole correlations. Sci. China Phys. Mech. Astron. **66**, 252011 (2023). https://doi.org/10.1007/s11433-022-2045-x
55. E.F. Zhou, X.Y. Wu, J.M. Yao, Multireference covariant density-functional theory for the low-lying states of odd-mass nuclei. Phys. Rev. C **109**, 034305 (2024). https://doi.org/10.1103/PhysRevC.109.034305
56. F.Q. Chen, Y. Sun, P.M. Walker et al., Mixing effects on K-forbidden transition rates from the 6^+ isomers in the $N = 104$ isotones. J. Phys. G **40**, 015101 (2013). https://doi.org/10.1088/0954-3899/40/1/015101
57. P. Ring, P. Schuck, *The Nuclear Many-Body Problem* (Springer-Verlag, New York, 1980)
58. P.W. Zhao, Z.P. Li, J.M. Yao et al., New parametrization for the nuclear covariant energy density functional with point-coupling interaction. Phys. Rev. C **82**, 054319 (2010). https://doi.org/10.1103/PhysRevC.82.054319
59. B. Bally, B. Avez, M. Bender et al., Beyond mean-field calculations for odd-mass nuclei. Phys. Rev. Lett. **113**, 162501 (2014). https://doi.org/10.1103/PhysRevLett.113.162501
60. D.L. Hill, J.A. Wheeler, Nuclear constitution and the interpretation of fission phenomena. Phys. Rev. **89**, 1102–1145 (1953). https://doi.org/10.1103/PhysRev.89.1102
61. S.J. Krieger, P. Bonche, H. Flocard et al., An improved pairing interaction for mean field calculations using skyrme potentials*. Nucl. Phys. A **517**, 275–284 (1990). https://doi.org/10.1016/0375-9474(90)90035-K